

PAPER

## Analyses of the plastic deformation of coated conductors deconstructed from ultra-high field test coils

To cite this article: Xinbo Hu *et al* 2020 *Supercond. Sci. Technol.* **33** 095012

View the [article online](#) for updates and enhancements.



**IOP | ebooks™**

Bringing together innovative digital publishing with leading authors from the global scientific community.

Start exploring the collection—download the first chapter of every title for free.

# Analyses of the plastic deformation of coated conductors deconstructed from ultra-high field test coils

Xinbo Hu<sup>1</sup> , Michael Small<sup>1,2</sup>, Kwanglok Kim<sup>1</sup>, Kwangmin Kim<sup>1</sup>, Kabindra Bhattarai<sup>1,2</sup>, Anatolii Polyanskii<sup>1</sup> , Kyle Radcliff<sup>1</sup>, Jan Jaroszynski<sup>1</sup> , Uijong Bong<sup>3</sup> , Jeong Hwan Park<sup>3</sup>, Seungyong Hahn<sup>1,3</sup>  and David Larbalestier<sup>1,2</sup> 

<sup>1</sup> NHMFL, Florida State University, Tallahassee, FL, United States of America

<sup>2</sup> Department of Mechanical Engineering, FAMU-FSU College of Engineering, Tallahassee, FL, United States of America

<sup>3</sup> Department of Electrical and Computer Engineering, Seoul National University, Seoul, Republic of Korea

E-mail: [xhu@asc.magnet.fsu.edu](mailto:xhu@asc.magnet.fsu.edu)

Received 5 May 2020, revised 21 June 2020

Accepted for publication 20 July 2020

Published 12 August 2020



## Abstract

REBCO coated conductors are now being used for building very high-field magnets with large electromagnetic stresses, both expected ones due to transport current  $\vec{J} \times \vec{B}$  stresses and additional stresses resulting from the large screening currents inherent in wide tapes. *Post mortem* analyses of several recent test coils operated above 40 T show that significant conductor plastic deformation occurs, even for *JBR* stresses well below the  $\sim 1$  GPa yield of the Hastelloy substrate of the conductor. To investigate these deformation mechanisms, conductors were unwound after coil test and carefully examined with respect to their length-wise  $I_c$  which revealed many areas of local damage. Regions of interest were examined by metallographic cross-section, Hall microscopy, magneto-optic imaging and scanning electronic microscopy. Important damage frequently occurred to the outer edges of pancakes in the coil ends, which were often plastically deformed over the whole turn circumference, especially when this outer edge was a slit edge. Internal conductor damage was also seen, especially delamination between the buffer and REBCO layers at slit edges. Careful sectioning of the tape at  $\sim 10$  mm intervals showed that the plastic deformation of the turns was complex and variable around the turn circumference, with tape cross-sections that exhibited continuous shape change in the outer turns. The bending center line of tapes often shifted from the tape center line toward the edge closest to the coil center, indicating asymmetric effects of transport and screening current stresses across the conductor width. A surprising and vital result is that damage was prevalent when the slit edge was also the edge at which transport current flowed. This damage was absent when the transport current flowed at the not-slit edge, implying great sensitivity of the effect of screening current stresses to localized conductor damage.

Keywords: ultra-high-field, no insulation, screening current

(Some figures may appear in colour only in the online journal)

## 1. Introduction

The high critical current density  $J_c$  of REBCO CCs at high-field ( $>30$  T) and low temperature (4.2 K) [1, 2] makes them suitable for building ultra-high-field (UHF) magnets

well beyond the capabilities of  $\text{Nb}_3\text{Sn}$ . Besides the 32 T all-superconducting user magnet at the NHMFL [3–5], a project at the Francis Bitter Magnet Laboratory (FBML) that aims to build a 1.3 GHz NMR magnet also adopts REBCO CCs as its conductor [6, 7]. In the quest for ever higher field with

CCs, 35.4 T was achieved by a layer-wound insert coil in a background field of 31 T in 2011 [8] and an all-REBCO magnet using the no insulation (NI) winding technology achieved 26.4 T in 2016 [9]. Very recently, the Institute of Electrical Engineering in China achieved 32.35 T with an NI insert in a 15 T background [10], and a large bore insert (38 mm inner diameter) wound with metal-as-insulation technique achieved 32.5 T in an 18 T background in Grenoble [11]. However, many challenges still exist in translating test coils into real magnets. For example RIKEN built two 28 T insert magnets from layer-wound REBCO but both damaged themselves in spontaneous quenches [12]. Tohoku University built a REBCO insulation coil and achieved 23.6 T in a 14 T background, where it quenched and was damaged [13]. FBML's 18.8 T insert coil also degraded during spontaneous quench in its first test [14]. In spite of all these degradations, there is also one user magnet that has been in service for several years *without any quenches*. The 18 T 70 mm all-REBCO magnet was designed and constructed by SuNAM and Seoul National University, and has been continuously operated at the Institute of Basic Science since October 2017 [15].

With the development of more forms of Coated Conductors, especially those with the thin 30  $\mu\text{m}$  substrate, more compact coils of higher winding current density can be made. Alloying such thin-substrate tape with the NI winding technique [16], we have now made three test coils that can operate in the 50 mm warm bore of a 31 T Bitter magnet at the NHMFL to explore how high a field we could make. They are named little big coils (LBCs), Little because of their small physical size (35 mm OD, 14 mm ID and 50 mm length) and Big because they can create a big field when immersed in the 37 mm diameter cryostat of the 31 T magnet. LBC1 and LBC2 were tested in 2016 and early 2017, and reached 40.2 and 42.5 T, respectively. LBC3 made a world record DC field of 45.5 T in August 2017 [17]. All three coils were driven to spontaneous quench by ramping the transport current slowly in a static 31 T external field. All three coils exhibited some degradation after quench, LBC1 to the top and bottom pancakes, while LBC2 and LBC3 showed more general degradation. In general, the higher the final field, the more degradation was observed after each quench. In this paper, we discuss the nature of this degradation based especially on a detailed *post mortem* obtained by running the tapes through our continuous critical current measuring device, YateStar [17, 18].

## 2. Experimental details

A key feature of our three LBC test coils that achieved more than 40 T is that they showed unexpected damage that incited us to do extensive *post mortem* analyses that form the subject of this paper. For the second highest field coil (LBC2), the conductor was visually inspected and run through YateStar at 77 K only after test so as to get a high-resolution map of the superconducting properties of the tape. Recognizing the damage of LBC1 and 2, we decided to measure the tapes of LBC3 before and after the 45.5 T test. YateStar provides two types

of lengthwise critical current information  $I_c(x)$ , the first being transport  $I_c$  at  $\sim 2$  cm resolution for  $B\parallel c$  at fields up to 1 T and for  $B\parallel ab$  at fields up to 0.6 T. This biaxial characterization allows study of the uniformity of the dominant precipitate vortex pinning mechanisms in the tape, as well as of interruptions to the current-flow cross-section due to, for example, substrate or buffer defects. YateStar also has a 7-element Hall probe array between the above two magnets and, in the absence of transport current, this provides information about the lengthwise induced currents and the transverse uniformity on a scale of order 1 mm. After high-field test of all three coils, each of the 12 pancakes was unwound, inspected and run through YateStar. Because some of the tapes were deformed during their test above 40 T, larger but still small tension ( $<10$  N,  $\sim 50$  MPa) than usual was applied to ensure proper tape transport during measurement. These scans showed that periodic degradations on some tapes were present after test and several such degraded regions were cut out for microscopic inspection, including magneto-optical imaging (MOI) which allows direct observation of the uniformity of current flow. Subsequently the Cu and Ag were etched away with APS-100 and  $(\text{NH}_4)_2\text{S}_2\text{O}_8$  respectively so as to allow check by scanning electronic microscopy (SEM) of the integrity of the REBCO layer, especially at the tape edges.

To assess the lengthwise fluctuations of the plastic deformation of the tapes after high field test, cross-sectional views of the tapes  $\sim 10$  mm apart, before and after the high field tests, were obtained from outer turns of  $\sim 110$  mm length from pancakes 1, 2, 6, 11 and 12 of LBC3. During the metallographic sample preparation, great care was taken to preserve the shape integrity of the tapes. The cross sections were mounted in a two-step procedure. Initially, a 10 mm tall puck of a graphite and mineral-filled phenolic thermoset was made into which slots were milled as a guide for the tapes. The 10 mm long sections were inserted with their cross sections flush with the bottom of the puck. Epoxy was then poured over the mount and time allowed for hardening. The puck was then polished and imaged, repolishing sometimes being done in 1 mm increments to progressively reveal depth-dependent features. Images were taken by an Olympus light microscope.

The 4 mm wide tapes of all three coils were manufactured by SuperPower with 30  $\mu\text{m}$  cold-rolled Hastelloy substrate and 5  $\mu\text{m}$  of electroplated Cu on each side. They were delivered in twelve 20 m long pieces, all of them having at least one mechanically slit edge (front-slit or back-slit) and some having two slit edges (middle-slit).

The pancakes are numbered 1 to 12 from top (P1) to bottom (P12). They were wound with inner and outer diameters of 14 and 34 mm with their REBCO layers facing radially inward in order to create compressive bending strains. To define the pancake location in the coil, 'upper' and 'lower' refer to the vertical direction. 'Inner' and 'outer' refer to the radial position of the tape within each pancake. We take the plane between P6 and P7 as magnet center reference, and use 'inward' and 'outward' to define the orientations of the tape edges with respect to this central plane, particularly when we come to describe the important role played by the location of the slit edge(s).

### 3. Results

#### 3.1. Visual inspection and lengthwise $I_c$ characterization of tapes LBC2

Figure 1(a) shows photos of the evident rippling on one edge in unwound sections of tapes from LBC2 after test. The rippled edge is on the top for P1, P2, and at the bottom for P8 and P11, that is the edge pointing toward the coil end in each case. The rippling on P4 is less obvious and only exists on the bottom edge of the very outermost turns. Because so localized, it may be associated with proximity to the outer solder joint. The ripple period is defined by the image of P8 in the picture. Figure 1(b) shows the ripple period versus position along the tape length from inner to outer turns for P1. The fit line depicts the radially-varying circumferences of inner to outer turns and gives the tape thickness as  $\sim 48 \mu\text{m}$ , very close to the manufacturer's specification of  $45 \pm 4.5 \mu\text{m}$ . The periods match the circumferences for the inner and middle turns but the period drops and becomes more random for outer turns with radius larger than 14 mm.

Figure 2 shows the position dependence of  $I_c$  (77 K) of the tapes unwound from the LBC2 coil. In this case, because of the damage suffered by the tape, we preferred to avoid direct transport measurement and to deduce  $I_c$  values from the non-contact Hall probe array signal which was scaled to the transport  $I_c$  measured with  $B \parallel c$ , 0.6 T. The left ends of  $I_c(x)$  always correspond to the outer diameters of the pancakes. The degradations on the outer turns of P1, P2, P8, and P11 are related to rippling of the tapes, which all occur on the outer edges. The degradation of P4 is relatively smaller compared to the above pancakes. The  $I_c$  drops at the left end of each tape occur at the joints that connect the pancakes. The tape of the bottom pancake, P12, was damaged by a mounting screw that inadvertently penetrated into the winding during assembly. No other degradations were observed.

#### 3.2. Microstructural examinations of LBC2

Figure 3 shows 2D Hall magnetization maps that are quite non-uniform across 1 m lengths of the outer turns of P1 and P2 of LBC2. As a comparison, the inner turns of P12 has no obvious degradation and is relatively uniform. Many longitudinal drops in the signal are seen which correspond to cracking damage that we associate with excessive hoop strains. The maps clearly show more damage on the outer tape edges, which are also the slit edges, particularly for P1. For P2, there are apparent periodic degradations, whose period matches the circumferences of the outer turns. Although P1 presents similar transverse defects as P2, the periodicity is not so obvious and the degradation is more generally severe.

To better visualize the superconducting impact of the periodic damage of P2, a 10 mm long piece (the dashed rectangle in figure 3) was cut out for MOI and SEM. Figure 4(a) shows the light image, while (b) and (c) show the polarized light MO images (taken at 10 K, 120 mT after ZFC and 0 mT after FC in 120 mT, respectively). The degraded and superconducting regions are indicated in the images. The rough upper

edge of the sample indicates more damage than on the lower edge. A major defect penetrating about half the tape width is visible in the middle of the image. The Cu and Ag layers were then etched away to allow direct inspection of the REBCO layer itself by SEM. Figures 5(a) and (b) show top views of the upper and lower edges, which confirm that the irregular flux penetration of figure 4 occurs preferentially at the slit edge. The oblique curved cracks produced by slitting penetrate 20–25  $\mu\text{m}$  from the edge but are about three times longer (see figures 5(a) and (c)). In some places, the buffer layer is exposed and delaminated REBCO is observed at the edge (figure 5(a)). It is possible that the delamination between REBCO and the buffer layers is even more extensive than what can be seen in the image, given that the magnetic flux penetration of figure 4(b) occurs to half width of the tape. Longitudinal focused ion beam' bed sections of the damage are also of interest, as in figure 6. In the section made 10  $\mu\text{m}$  away from the slit edge (figure 6(a)), there is an extensive gap between the buffer and the REBCO layer. The much better connection to the Ag cap layer suggests a better adhesion of REBCO to the Ag than to the buffer layer. This observation also suggests that the real extent of delamination damage is not visible from purely topographic imaging of the bare REBCO layer. We conclude that companion MO images are more reliable in assessing the damaged areas because they directly image the fields generated by the induced screening currents of the REBCO layer. Figure 6(b), 15  $\mu\text{m}$  into the layer shows less damage but the layers are still far from perfect. The porous REBCO close to the buffer layers is unlikely to be able to carry supercurrent.

#### 3.3. Cross-sectional views of the plastic deformation in LBC3

For LBC2, we did not measure the tapes prior to winding them into the coil and so we lack the lengthwise  $I_c$  distribution of the tapes before test. However, for LBC3 analysis before and after test revealed that the conductor is better protected if the slit edge faces inwards [17]. Figure 7 shows a transverse cross-section of the as-received LBC tape with an evident camber. The arrows in figure 7(a) illustrate the measurements of width and height. Figures 7(b) and (c) are enlarged views of the slit and not-slit edge, respectively. The black arrows indicate the thin REBCO layer. On the slit edge side, the Hastelloy is not covered by REBCO for about 15  $\mu\text{m}$ , which is a sign of damage by the mechanical slitting (marked by a dark yellow arrow). The sputtered Ag covering is also not perfect, as indicated by the white arrow. More importantly, the exposed Hastelloy is slightly rounded, in contrast to the not-slit edge as indicated in the figure. All these pre-existing, as-delivered imperfections may make the slit edge more prone to delaminate, as shown in figure 6.

Figure 8(a) shows smoothed height contour maps of  $\sim 110$  mm long tape sections taken from P1, P2, P6, P11 and P12, while figures 8(b) and (c) show camber profiles made using the careful tape cross-section measurements of the type shown in figure 7(a). In these, the outer tape edge (i.e. that facing the end windings) is defined as  $y = 0$  mm. The interval between two cross-sections is about 10 mm, and the height numbers in-between are obtained by linear interpolation in

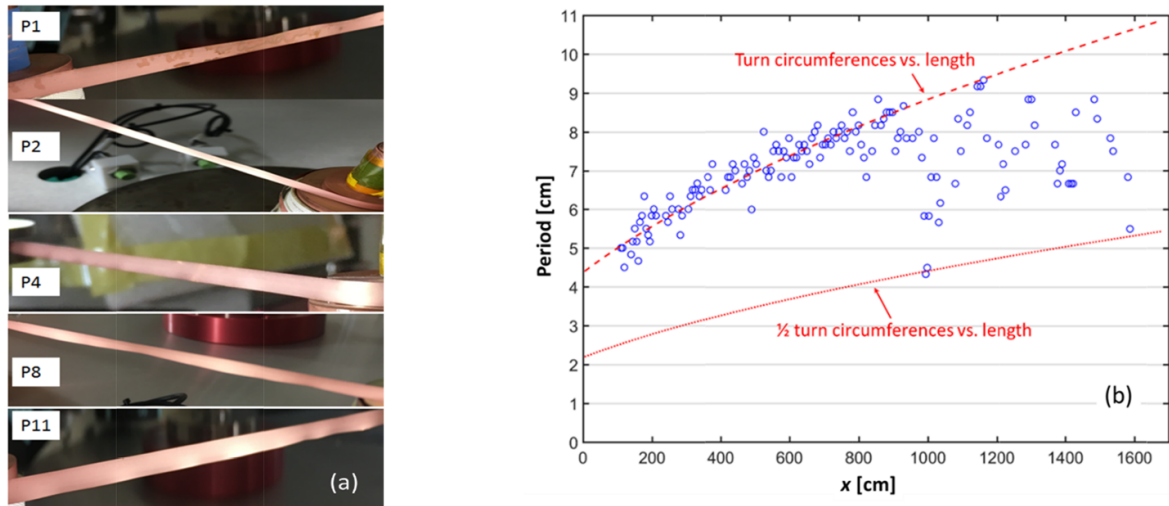


**Figure 1.** (a) Photos of short conductor lengths with one rippled edge unwound from the pancakes. The ripple period is marked by the double-headed arrow on P8. (b) Ripple period versus tape position from the inner to the outer turns of P1, LBC2. The fitting line is the circumference of inner to outer turns versus tape position. The tape thickness fit is  $48 \mu\text{m}$ , which is consistent with the manufacturer's  $45 \pm 4.5 \mu\text{m}$  specification. It can be seen that the ripple period is quite accurately the circumference up to  $\sim 900 \text{ cm}$  tape length but it becomes shorter and more variable for the outer turns.

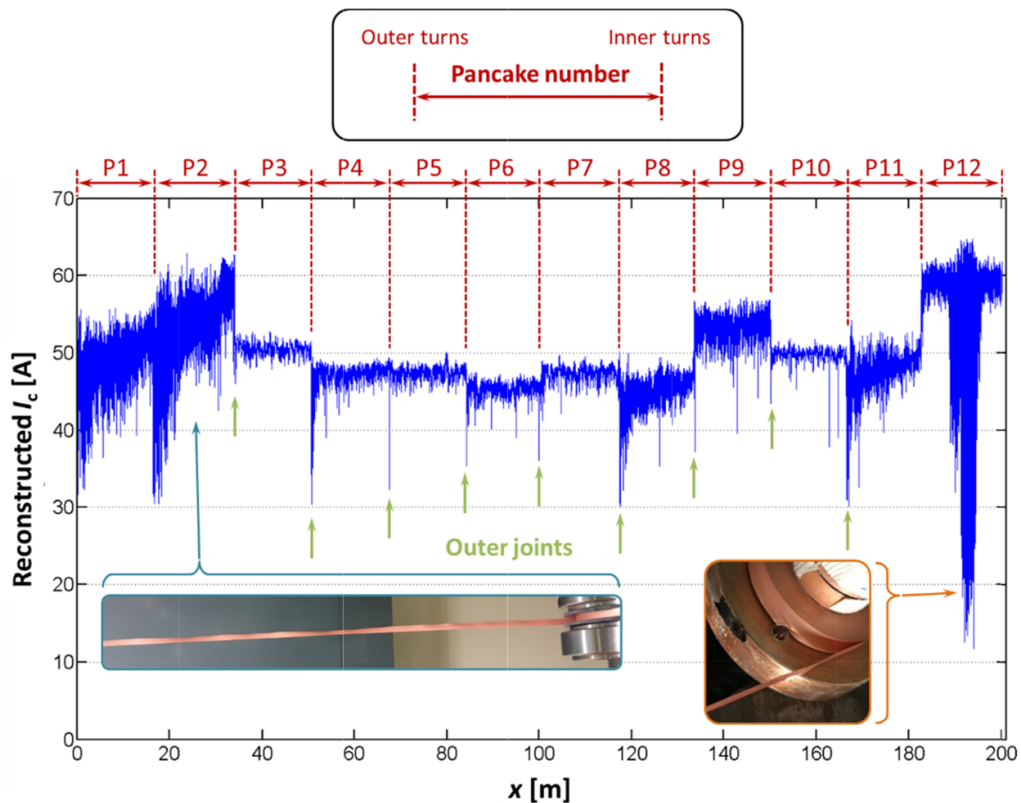


**Figure 2.** Position dependence of  $I_c$  (77 K) of the tapes after coil test which ended with one quench at 42.5 T. The reconstructed  $I_c$  derived from the Hall probe array is scaled to the transport  $I_c$  measured at  $B||c$ , 0.6 T. The tapes are connected in series from outer to inner turns. The sharp drops at pancake transitions are due to the degradation of the outer joints of the coil.

figure 8(a). It is immediately obvious that the 45.5 T test produced a variable plastic deformation of the tape, represented by a variable tape flattening that varies pancake to pancake and along the length and across the width. Thus the deformation is not azimuthally uniform as is normally assumed. Furthermore

the axis of maximum post-test tape deformation from end pancakes P1, P2, P11 and P12 is not on the geometrical center line of the tapes but shifted toward the edge facing the center of the coil, irrespective of the slit edge orientation. Central pancake P6 has a distinctly more symmetric flattening than

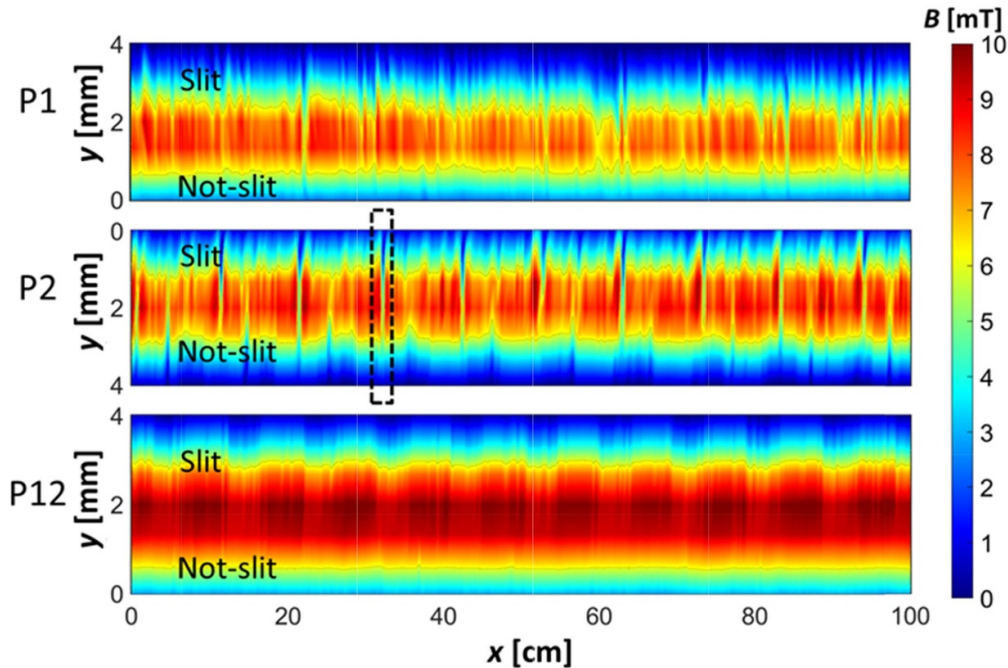


**Figure 3.** Two-dimensional magnetization maps of 1 m lengths of the outer turns of pancakes P1, P2 and the inner turns of P12 of LBC2. P12 was wound with tape from the same production run as that of P1 and P2 but has no obvious degradation. The dashed rectangular box is the region cut out for magneto-optical imaging in figure 4. Evident transverse damage is present in both P1 and P2 tapes but is much less obvious in P12.

the end pancakes and also has the greatest flattening, perhaps consistent with it having the greatest *JBR* stress and minimum screening current stress, as shown later in figure 12. However the most axially uniform deformation occurs in pancakes 2 and 11, a point we return to later in our discussion of the damage profiles and their relationship to the screening current distributions. Figure 8(b) shows the average camber flattening versus the tape width for the four end and one central pancake in (a). The tape curvature after winding with the same tension as for the LBC coils is also included; The slight lateral shift of the bending center is probably due to a winding misalignment, but the camber height is barely altered, making it clear that all of flattening seen in the deconstructed pancakes is a result of the UHF test, as also is the asymmetric deformation evident in figures 8(a) and (b). Figure 8(c) shows the maximum height versus its width position. Comparison of the average deformation of each 110 mm tape length to the maximum deformations shows that the maximum deflections are about 30% larger than the average (P12), providing yet more evidence for the highly localized, non-axisymmetric deformation of the tapes in the four end pancakes after reaching 45.5 T. Table 1 summarizes the deflection distributions of each section for each pancake; the smaller mean value ( $\mu$ ) means greater flattening of the REBCO tape, while the larger is standard deviation ( $\sigma$ ) the more is the deformation way. It is evident that shape profiles of P2 and P11 with slit edges facing toward the magnet center are much more uniform than those of the other pancakes, whose slit edges faced axially outward. We note also that P6 was the most flattened, which corresponds to our previous report on the periodic  $I_c$  degradations measured by Yate-Star [17] and our simulation results of the largest transport

**Table 1.** Standard deviations and mean values of the maximum height of each section in figure 8(a).

Pancake	P1	P2	P6	P11	P12
Standard deviation ( $\sigma$ , $\mu\text{m}$ )	13.1	3.48	11.4	4.19	13.5
Mean value ( $\mu$ , $\mu\text{m}$ )	57.0	61.5	51.0	63.9	66.0
$\sigma/\mu$ (%)	23.0	5.66	22.3	6.56	20.5

plus overcurrent stresses at P6. In general, the ‘upper’ pancakes (P1–P6) experienced larger flattening than the corresponding lower pancakes (P7–P12) as expected because the magnet quench initiated in P12, triggering larger induced overcurrents in the upper pancake coils during the quench.

#### 4. Discussion

The key issues that we encountered during our *post mortems* of our greater than 40 T LBCs are serious damage to end windings that cannot be explained by conventional transport current and induced overcurrent stress calculations and the concentration of the damage to the outer windings where  $|B|$  is lower but  $B_r$  is higher. To be more specific, most of the damage is related to the plastic deformation of the conductor. The Hastelloy substrates were permanently rippled on their slit edges, where edge cracks produced during slitting propagated across the REBCO layer, sometimes causing delamination at the REBCO-buffer layer interface. Furthermore we also found a very significant interaction between the orientation of the slit edge toward the magnet ends and the occurrence of damage. When oriented this way extensive damage was found,

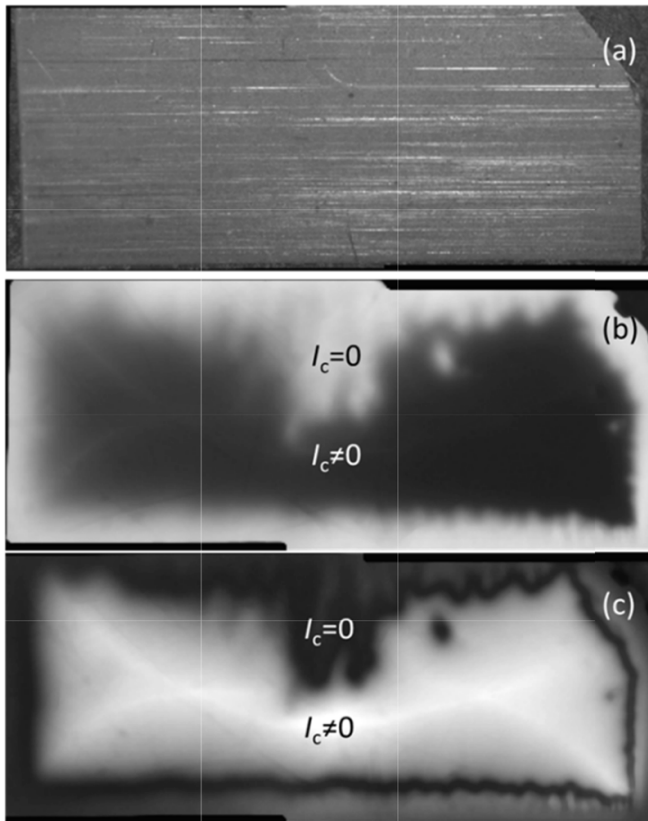


**Figure 4.** (a) Light micrograph image of the piece cut from tape P2 of LBC2 marked in figure 3. (b) The MOI image shows clear evidence of easy flux penetration at multiple places on the upper edge, which reaches approximately half of the tape width in the central region. By contrast the not-slit, lower edge is much more uniform. The upper right diagonal cut was made to mark the slit edge. The image was taken at 10 K in 120 mT perpendicular field after zero-field cooling (ZFC). (c) The corresponding image taken after field cooling (FC) in 120 mT, and then removing field at 10 K.

which could be largely suppressed by placing the (damaged) slit edge facing the magnet center. We believe that these damage patterns can only be explained by taking account of significant screening current stresses [17] and important interactions between the transport current and the damaged, slit edge of the tapes, as we now discuss in detail.

#### 4.1. Mechanical damage did not occur during coil construction

To assess the mechanical damage of the LBC pancakes, we have to evaluate all potential sources of overstress. First, we consider whether the winding procedures damaged the conductor  $J_c$  properties. Indeed, figure 9 compares YateStar scans before and after pancake winding. They show no observable change in  $I_c$  caused by the winding procedures, either locally or globally, even at the fine mm-scale resolution of the Hall probes. This tape was then rewound into P8 of LBC3, where it contributed to the achievement of 45.5 T. We accordingly conclude that damage observed in the deconstruction of the LBC coils was not caused by the coil winding process but by the subsequent test. We do note that the tapes were wound with

the REBCO on the inner winding radius side so as to maximize the compression on the REBCO layer. Testing tended to flatten this as-delivered camber significantly, as is clear in the cross-sections of figure 8.

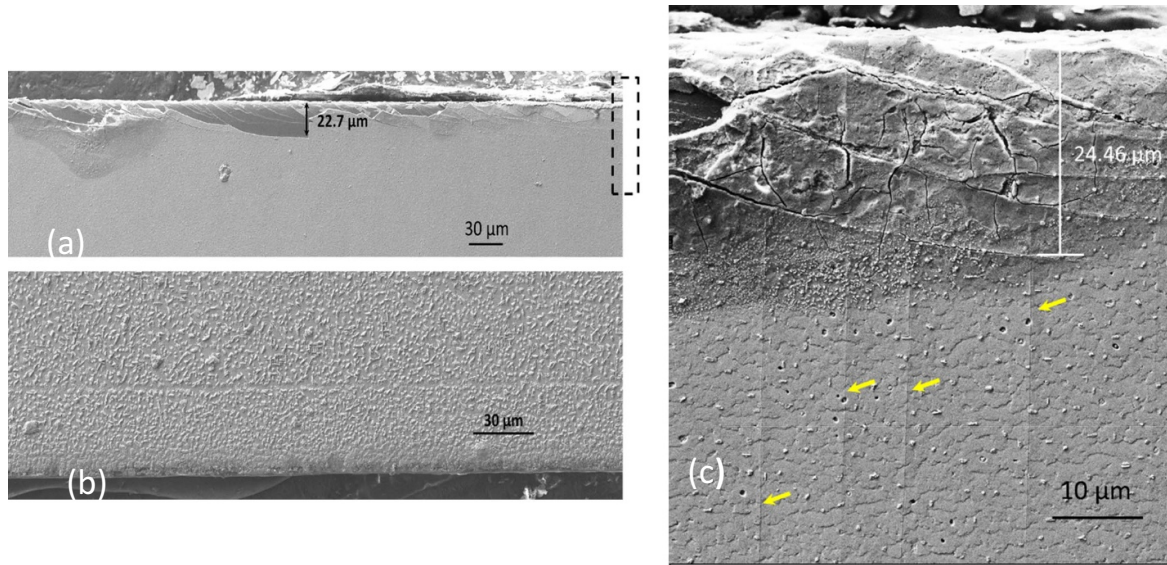
#### 4.2. Stress–strain characteristics of the conductor

Figure 1 shows that one obvious result of our *post mortem* investigation is that some pancakes were significantly and inhomogeneously plastically deformed by energization or by the subsequent quench. Figure 10 shows the 77 K stress–strain curves of two samples of the as-received tapes made with an attached extensometer, both giving identical results within the experimental points. The first yield event occurs at  $\sim 400$  MPa, presumably where the  $\sim 10$   $\mu\text{m}$  of Cu and 4  $\mu\text{m}$  of Ag yields. A definable yield stress of the whole tape occurs at  $\sim 900$  MPa and the 0.2% yield strength occurs at  $\sim 1.02$  GPa. The linearized elastic modulus below 400 MPa is 192 GPa, declining to  $\sim 170$  GPa above the plastic yield regime of Cu and Ag. Based on measurements of other SuperPower tapes we expect the 4 K properties to be 5%–10% higher. By contrast the maximum calculated transport current hoop stress  $JBR$  was 750 MPa which occurs in P10 of LBC3, values which are clearly not high enough to plastically deform the Hastelloy, leading us to conclude that there must be additional stresses to cause the observed plastic deformation damage.

#### 4.3. Role of transport current, induced quench overcurrent and screening currents in causing the conductor plastic deformation behavior

From the two key observations that (1) coil winding does not damage the tapes and (2) the correlation that larger magnetic field and transport current produces more plastic rippling, we conclude that the plastic rippling originates from electromagnetic sources which have four possible components: (1) two current density components, azimuthal ( $J_\theta$ ) and radial ( $J_r$ ); and (2) two magnetic field components, radial ( $B_r$ ) and axial ( $B_z$ ). The radial current density  $J_r$  is unique to a no-insulation pancake coil as it represents the turn-to-turn leakage current. However, we assume this to play a negligible role here due to the very slow ramping rate ( $0.5 \text{ A s}^{-1}$ ) of LBC and small self and mutual inductance with the external 31 T resistive magnet. We now discuss the other potential sources in turn.

**4.3.1. Transport current.** It is well understood that a magnet experiences magnetic hoop stress by a Lorentz force interaction between the transport current and the magnetic field. Since the LBC coils were ‘dry-wound’, each turn was essentially ‘self-supporting’ during the entire operation of each LBC, allowing the transport current hoop stress to be estimated by  $JBR$ , where  $J$ ,  $B$ , and  $R$  represent transport current density, axial magnetic field, and radius of each turn [19]. According to our  $JBR$  calculations of LBC sitting in the 31 T outsert field, the stress in each pancake increases as the radius increases, making the peak  $JBR$  stress occur near the outermost turn. We note that about three extra turns were wound onto each pancake after the pancake-to-pancake joints were made. The



**Figure 5.** (a) and (b), top views of the upper (slit) and lower (not-slit) edge of the sample in figure 4 after removing Cu and Ag. (c) Enlarged view of the box with dashed line in (a). The transverse cracks indicated by the arrows might be caused by stress-concentrations. The slitting cracks (slightly curving cracks at  $\sim 30^\circ$  to the tape edge) can be clearly seen in both the REBCO and buffer layers, and usually extend 20–25  $\mu\text{m}$  in depth from the edge. The not-slit edge presents a large density of  $a$ -axis grains, but no cracks.

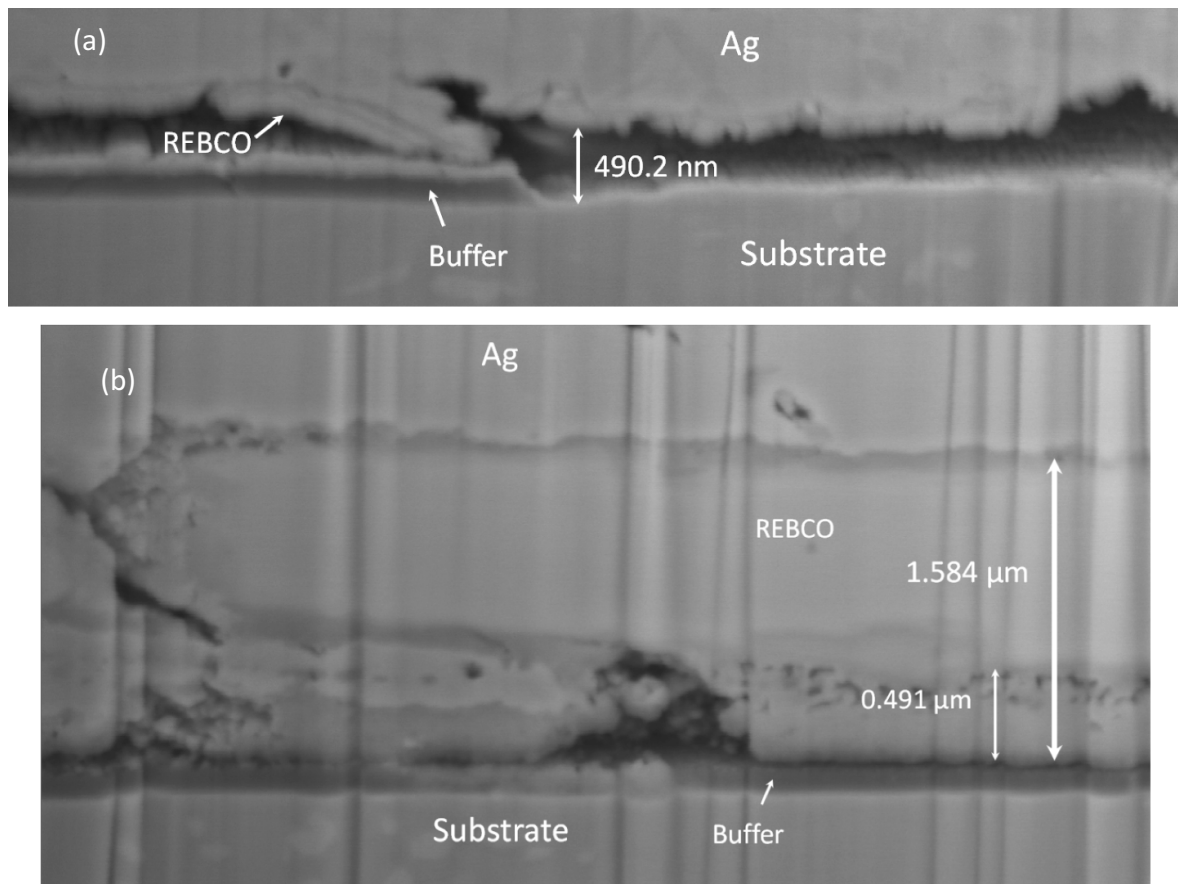


**Figure 6.** Longitudinal cross-sectional views (a) 10  $\mu\text{m}$  and (b) 15  $\mu\text{m}$  away from the damaged, slit edge. REBCO is clearly delaminated from the buffer at 10  $\mu\text{m}$  from the edge. The bottom of REBCO layer is porous, while the top is more compact.

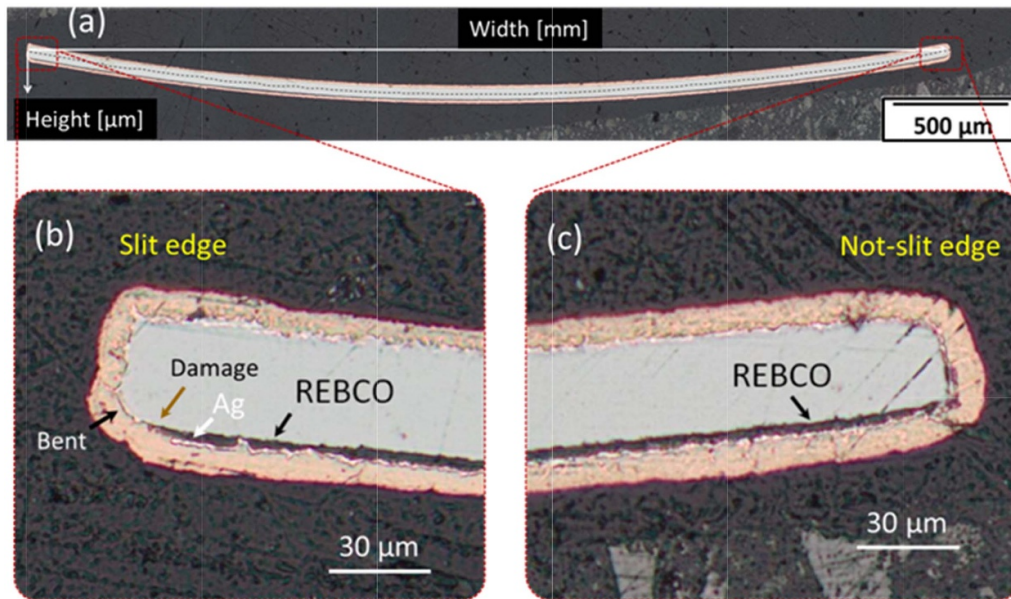


**Figure 7.** (a) Transverse cross-sectional views of the as-received tape and (b) and (c), enlarged views of the two edges. The arrows in (a) illustrate how the width and camber height are defined. The slit edge shown in (b) has REBCO missing over  $\sim 15 \mu\text{m}$  at the very edge, a result of the mechanical slitting during manufacturing.

minor role of this overband is accounted for in the calculations of figure 12(c). We note that the post-test damage seen in figure 2 for LBC2 and already reported for LBC3 [17] is completely consistent with this ‘larger-stress-at-larger-radius’ *JBR* calculation.

**4.3.2. Induced overcurrent.** A second important factor is the ‘induced overcurrent’ that is often observed in a no-insulation HTS coil during rapid quench. Using our lumped circuit code (which does not take account of screening currents), we simulated the quench propagation within LBC3 [17], the simulated voltages of each pancake agreed reasonably well with the measured voltages on each pancake. Indeed we found that these induced overcurrents corresponding to these voltages did generate a significantly higher calculated peak stress of  $\sim 900 \text{ MPa}$ , a value now rather close to the tensile yield stress of figure 10, at least for the middle pancakes where the largest stresses are predicted. As figure 11 shows, P12 initiated the quench, the other pancakes then quenching sequentially from bottom to top. We conclude that these overcurrent stresses are certainly important but we return to the fact that the most characteristic plastic damage to the LBC coils occurs in the end pancakes where the *JBR* stresses are lower. Figure 11 also takes account of the compressive winding strain on the conductor which reduces the overcurrent strains in the end pancakes 1,2, 11 and 12 to  $<0.4\%$ . Such a strain is essentially elastic according to figure 10, which means that the plastic rippling cannot be fully explained by taking account only of transport and overcurrent stresses.

**4.3.3. Screening current.** The third source of electromagnetic stress arises from screening currents generated by placing LBC in the 31 T field of the outer magnet prior to

transport current ramping to  $>40 \text{ T}$ . LBC1 and 2 quenched during holding at field while the coil ends were slowly heating in the He bubble generated by joint dissipation, while LBC3 quenched during slow ramping of the transport current. Thus no controlled current ramp-down was performed for any of the coils and the overcurrent stresses complicate consideration of the screening currents. However, in post-LBC3 tests of three single-pancake coils in 31 T background [17], the current was ramped up and down from 0 to 250 A, and also cycled between 225 to 250 A multiple times without quench. It turned out that only coil B placed in the position of PC 1 with strong radial field and with its slit edge facing the magnet end was plastically rippled, just as was seen for similarly oriented pancakes in LBC2 and 3. In complete consistency with the LBC coils, its coil A counterpart with slit edge facing the magnet center was undamaged. The electromagnetic damage seen in the YateStar scans of LBC2 and 3 was identical, except for the increasing frequency of current drops seen in figure 2 at higher radius that we attribute to quench overcurrent strains and much more obviously in the LBC3 traces in reference 17. We conclude that these observations all support the conclusion that the conductor can be plastically rippled without any induced overcurrent in a large background field. The result also suggests that the cycling of transport current has no obvious effect on the current/stress distributions except slightly shifting the electric center and the current distributions were mainly dominated by the strong background field. These results persuade us that the key cause of plastic rippling damage is the overstress caused by screening currents.

#### 4.4. Local damage due to pre-existing micro cracks and their propagation

We now wish to explicitly link the macroscopic plastic rippling observed on outer slit edges evident in figure 1 and the micro-

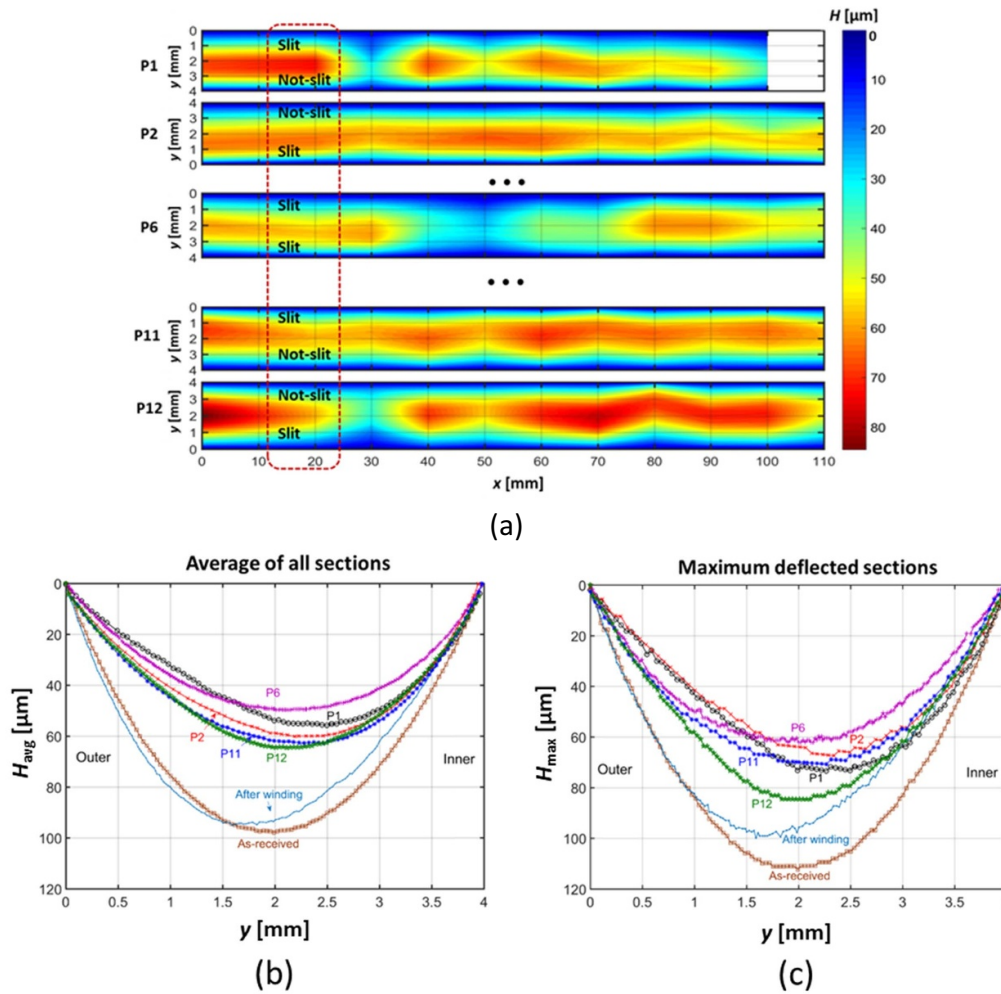


**Figure 8.** (a) Contour map reconstructed from the 10 mm-spaced cross-sectional views. The images were digitized, and the transverse sampling step in the  $y$  direction is about 0.03 mm. (b) Average height and (c) maximum height versus width position. The after-winding sample was cut from a coil never energized. The stresses of testing to 45.5 T partially flattened the tape and also moved the bending center of the tapes toward the magnet center, regardless of the slit edge orientation. The data on the as-received tape was averaged from three different pieces.

scopic interruptions to supercurrent flow seen in the Hall array and MO images of figures 3 and 4 with the damaged REBCO layers and especially the REBCO-buffer layer interface cracking seen in figures 5 and 6. An important issue is why these effects occur ONLY when the slit edge is facing the magnet ends.

As seen in figure 8, these thin ( $30 \mu\text{m}$  Hastelloy) tapes come with a significant camber from the manufacturer and this camber is first slightly flattened by winding but then much more markedly flattened and made aperiodic and asymmetric by the magnet test, thus implying that the local stress responsible for deformation is locally varying both along and across the tape. The deformed tapes ripple at the slit (outer) edges in periods matching the circumferences of coil turns (figure 1), suggesting an asymmetric deformation of the tape with a kind of buckling instability which occurs once per turn.  $I_c(x)$  of some pancakes also shows periodic  $I_c$  degradations (figure 3), which are probably results of stress concentrations in the radial direction of pancakes. MO (figure 4) and SEM images (figure 5(c)) reveal locally variable transverse cracks

in these degraded regions. Especially the MO images make clear that the damage extends mm into the tape well beyond the  $\sim 25 \mu\text{m}$  deep damage seen in the as-delivered slit edge (figure 5). As noted above, it is very significant that identical behavior was seen in the never-quenched, single-pancake coil A tested in P1 position in the 31 T magnet [17]. A distinct feature is that slitting cracks are present in the outer edges and propagate transversely across the tape to hundreds of microns depth, a damage certainly enhanced by plastic buckling of the outside edge. We believe this to be strongly linked to the screening currents present in the coil at the start of the transport current ramp. Figure 8 cross-sections of pancakes in LBC3 show that all the tapes from the end pancakes have their bending centers shifted toward the coil center, no matter how their slit edges are oriented. Since the increasing transport current displaces the initially symmetric screening currents by flowing in the same direction at the outer edges, the displacement of the axis of curvature toward the coil center agrees with a higher transport current deformation on the outer edges.

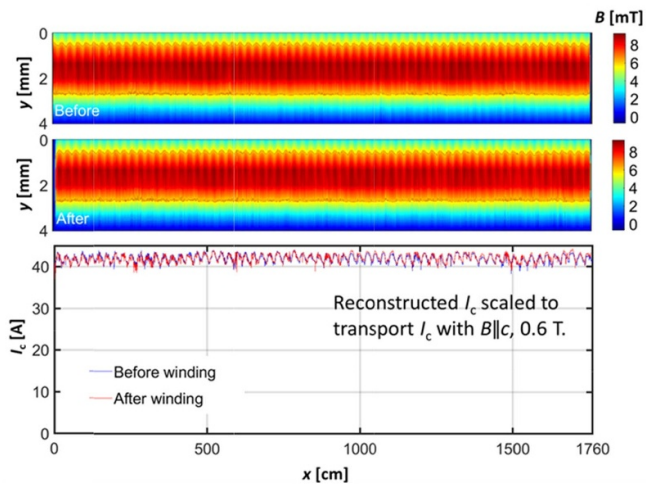


**Figure 9.** Comparison of a tape before and after winding into P8. The  $I_c$  values are reconstructed from the magnetization maps and scaled to the transport  $I_c$  for  $B \parallel c$ , 0.6 T at 77 K. There is no observable damage made by winding (and unwinding).

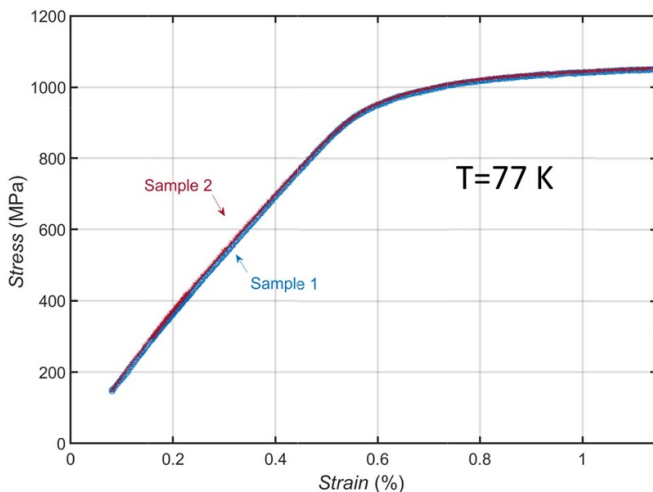


**Figure 10.** Stress–strain curve of as-received tapes at 77 K. The maximum  $JBR$  hoop stress of any pancake was 750 MPa in central pancakes P10 in LBC3.

We note that there are also aperiodic  $I_c$  degradations in the deformed tapes. Just as the MO image (figure 4) shows, the actual degraded region extends much further into the conductor than is revealed by the SEM images of the as-delivered slitting cracks. The longitudinal cross-sectional views in figure 6 show that delamination of the REBCO-buffer layer can occur, even if appearing undamaged in a top view. A plausible explanation is that the combined transport current and screening electromagnetic stresses operating in the REBCO layer can only be safely supported by excellent bonding between all components in the multi-layer tape. The slitting cracks visible in the REBCO layer probably hide much larger delamination associated with the weak bond between the REBCO and buffer layers. The clear message of both LBC2 and 3 is that the orientation of the slit edge is very significant and that both rippling and cracking damage correlates

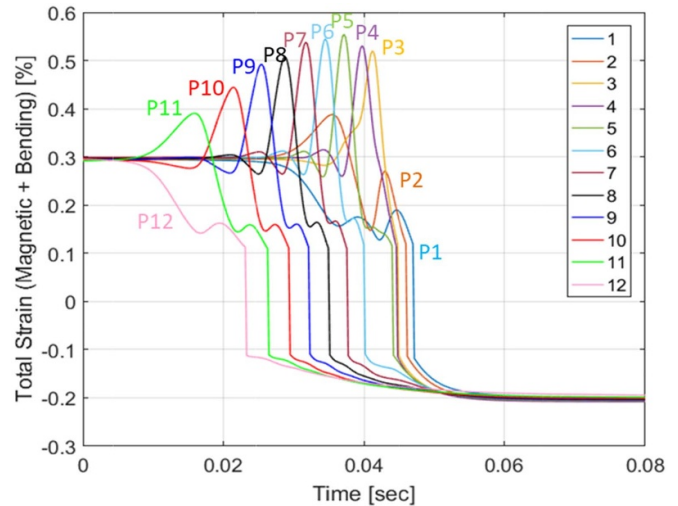


**Figure 11.** The magnetic plus compressive bending strain versus time during quench for LBC3. The total strain includes the magnetic hoop strain and the compressive bending strain.

to transport current flowing at the slit edge. As is well known from simulations, current streamlines are strongly distorted around cracks or other interruptions to current flow where the local electric field is greatly enhanced [20, 21]. Since the transport current penetration is driven by the electric field generated by the power supply, it is easy for local damage, whether periodic or aperiodic, to make major changes to the decaying screening currents, making their enhancement to the electromagnetic stress very specific to the local environment. It now becomes much more reasonable that the slit edge can be undamaged when it is turned to face the magnet center. According to the Bean model, there should be two streamlines of opposite-flowing current for the end pancakes exposed to strong radial fields ( $B_r$ ), and the streamlines in the outer edges should have the same direction as the transport current [22]. Thus, the outer edges experience a hoop stress expansion and the inner edges a compression. We did indeed look for damage at the inner edges but did not find it but buckling of this edge in test coils operating at lower stresses and lower fields has recently been reported [23]. The explanation offered is the plausible one that the inner edge compression is plastically unstable. In our case, the much larger tensile stresses in the outer edges may stabilize the inner edges since the maximum tensile stresses in the RIKEN test coil were  $<400$  MPa even with significant screening current amplification ( $\sim 4$ ) [23].

#### 4.5. The beneficial effects of incorporating screening current stress into the simulations

Figure 12(a) summarizes the plastic rippling behavior of all pancakes in the three LBC series; LBC1 reached a quench field of 40.2 T, while LBC2 quenched at 42.5 T and LBC3 achieved 45.5 T. The short red lines in LBC2 and LBC3 mark the slit edges of the pancake coils. It is apparent that more pancake coils experienced plastic rippling as LBC reached a higher field. However, almost all the pancakes with their single slit edge facing inward, i.e. front-slit or back-slit tapes, survived

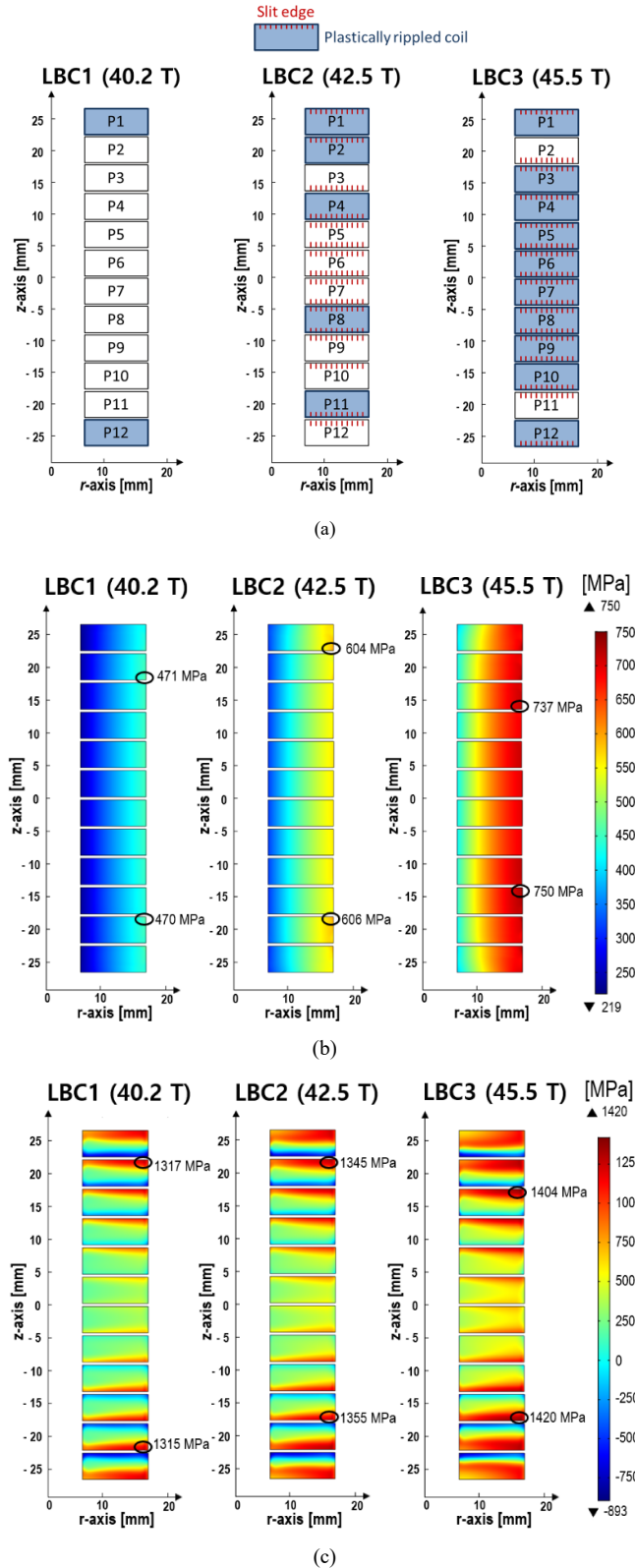


**Figure 12.** (a) A summary of the observed plastic rippling behavior of all pancake coils of the LBC series showing where mechanical rippling deformation was observed in the *post mortem*. The slit edges are marked by short red lines in LBC2 and LBC3. Slit edge positions were not controlled in LBC1. (b) Calculated hoop stress distribution of LBC1-3 at their peak fields without considering screening currents. (c) Calculated hoop stress of the LBC series at their full fields with transport and screening currents considered: LBC1 that reached 40.2 T; LBC2 at 42.5 T; and LBC3 at 45.5 T. The maximum stresses are circled in each figure.

without damage except P4 in LBC2, which shows a minor  $I_c$  degradation in its outermost turns, as shown by the Yate-Star scans in figure 2. Figure 12(b) shows the *JBR* hoop stress distribution of LBC1-3 at their peak fields without considering screening currents. We used the ‘measured’ dimensions of each pancake coil for the stress calculation. As a result, the peak stress was obtained in those pancake coils away from the magnet center as indicated in figure 12(b), which is barely different from the peak stress in central pancake coils. In any cases, the *JBR* stress values in all LBC series are incapable of generating the plastic rippling seen in figure 1. Figure 12(c) shows our simulations of the magnetic stress of the three LBC series at their peak quench fields. The so-called ‘index’ model with  $n = 21$  was adopted to model the non-linear  $E$ - $J$  characteristics of the REBCO tapes and domain homogenization and the 2D edge element formulation were adopted so as to be able to simulate both transport and screening currents simultaneously [24]. Recently several groups have reported similar simulations of screening current stress for various REBCO coils [23, 25–27]. A common feature is that none is yet numerically perfect. We thus offer our calculation more as a depiction of the very important redistribution of stress which occurs when screening current stresses are taken account of rather than an accurate calculation of the stress. Like the above model calculations, it appears too that our calculation overestimates the stress in the presence of screening currents.

Figure 12(c) includes the screening currents and shows that the peak local stress occurs not in the central windings where *JBR* is maximum but in the end windings with a peak value exceeding 1.4 GPa (P3 and P10, LBC3), which appears to be unreasonable as it far exceeds the yield and perhaps even the ultimate tensile stress of Hastelloy at 4.2 K. In addition, P3 and P10 of LBC1 and LBC2 survived all tests, including the quenches. But on the other hand, the calculations also show that the total current densities (transport + screening) of end pancake outer edges where the transport current preferentially flows are always larger than those at the inner edge where the residual screening current flows. These simulations correspond qualitatively to our *post mortem* observations: (1) the rippling plastic deformation of the REBCO tapes always occurs at the outer edge; (2) the bending center of end pancake tapes always moved toward the magnet centers, no matter how the slit edges were oriented.

An important and interesting failure of our screening current model is the inability of the stress calculations to account for the lack of damage seen in pancakes 2 and 11 of LBC3 when pancakes on either side (P1 and 3 and P10 and 12) are strongly damaged, the damage being both macroscopic rippling and the edge damage that makes important, aperiodic reductions to the local  $J_c$ . As noted previously, the outer edge is where the transport current enters. Our view is that current flow is relatively smooth in the not-slit edge because of its small defect population (mainly  $a$ -axis grains). But when the damaged edges lie in the transport current path, local distortion of the current stream lines and significant enhancement of the local electric field occurs, apparently magnifying the effects of the pre-existing slitting damage. This conjecture, supported both by simulations [20, 21] and observations of

constricted current flow at artificial defects [28] and by funneling of current between misaligned grains [29] suggests that significantly greater attention needs to be paid to the slitting process used for so many REBCO tapes. Although the damage observed here all occurred during a single test cycle of each coil, it is easy to predict that fatigue conditions could considerably worsen performance. It seems clear that greater attention must be paid to the whole slitting process and perhaps to addressing whether it is possible to enhance the bonding strength of the REBCO to its buffer stack.

## 5. Conclusions

Two UHF insert coils were deconstructed and analyzed after quenching at 42.5 and 45.5 T, respectively. Plastic rippling degradations were observed in both coils in the edges further away from the coil center. The deformation period matches the circumferences of the coil turns. SEM images confirm that all degraded edges occur at slit edges containing pre-existing micro-cracks. Transverse cracks were observed in places with periodic  $I_c$  dropouts, suggestive of strong stress concentrations. Delamination of the REBCO-buffer interface was also observed, even when the top REBCO surface appeared good. This poorly understood delamination may play a general role in coated conductor  $I_c$  degradation, as was well revealed here by MOI. Cross-sectional views of pancakes from LBC3 showed asymmetric deformation of the tapes and movement of the bending centers toward the magnet center for the end pancakes with more symmetric flattening for a central pancake. All these observations support a large role for screening current stresses, which appear especially harmful when the transport current is flowing along the slit (i.e. damaged) edge.

## Acknowledgements

This work was performed at the National High Magnetic Field Laboratory in Tallahassee FL which is supported by the National Science Foundation under Cooperative Agreement DMR-1644779 and by the State of Florida. The works by U. Bong, J. H. Park and S. Hahn were supported by the National Research Foundation of Korea as a part of Mid-Career Research Program (No. 2018R1A2B3009249). We are very grateful to colleagues in the REBCO R&D program at the lab who gave much discussion and support in this work.

## ORCID iDs

Xinbo Hu  <https://orcid.org/0000-0002-6553-3647>

Anatolii Polyanskii  <https://orcid.org/0000-0002-5977-5324>

Jan Jaroszynski  <https://orcid.org/0000-0003-3814-8468>

Uijong Bong  <https://orcid.org/0000-0002-5861-8669>

Seungyong Hahn  <https://orcid.org/0000-0002-4511-4162>

David Larbalestier  <https://orcid.org/0000-0001-7098-7208>

## References

- [1] Xu A, Jaroszynski J J, Kametani F, Chen Z, Larbalestier D C, Viouchkov Y L, Chen Y, Selvamanickam V and Xie Y Angular dependence of  $J_c$  for YBCO coated conductors at low temperature and very high magnetic fields *Supercond. Sci. Technol.* **23** 014003
- [2] Xu A, Delgado L, Khatri N, Liu Y, Selvamanickam V, Abraimov D, Jaroszynski J, Kametani F and Larbalestier D C 2014 Strongly enhanced vortex pinning from 4 to 77 K in magnetic fields up to 31 T in 15 mol.% Zr-added (Gd, Y)-Ba-Cu-O superconducting tapes *APL Mater.* **2** 046111
- [3] Markiewicz W D *et al* 2012 Design of a superconducting 32 T magnet with REBCO high field coils *IEEE Trans. Appl. Supercond.* **22** 4300704–4300704
- [4] Weijers H W *et al* 2014 Progress in the development of a superconducting 32 T magnet with REBCO high field coils *IEEE Trans. Appl. Supercond.* **24** 1–5
- [5] Weijers H W *et al* 2016 Progress in the development and construction of a 32-T superconducting magnet *IEEE Trans. Appl. Supercond.* **26** 1–7
- [6] Iwasa Y, Bascuñán J, Hahn S, Voccio J, Kim Y, Lécresse T, Song J and Kajikawa K 2015 A high-resolution 1.3-GHz/54-mm LTS/HTS NMR magnet *IEEE Trans. Appl. Supercond.* **25** 1–5
- [7] Bascuñán J, Hahn S, Lécresse T, Song J, Miyagi D and Iwasa Y 2016 An 800-MHz all-REBCO insert for the 1.3-GHz LTS/HTS NMR magnet program #x2014; a progress report *IEEE Trans. Appl. Supercond.* **26** 1–5
- [8] Trociewitz U P, Dalban-Canassy M, Hannion M, Hilton D K, Jaroszynski J, Noyes P, Viouchkov Y, Weijers H W and Larbalestier D C 2011 35.4 T field generated using a layer-wound superconducting coil made of (RE)Ba<sub>2</sub>Cu<sub>3</sub>O<sub>7-x</sub> (RE = rare earth) coated conductor *Appl. Phys. Lett.* **99** 202506
- [9] Yoon S, Kim J, Cheon K, Lee H, Hahn S and Moon S-H 2016 26 T 35 mm all-GdBa<sub>2</sub> Cu<sub>3</sub> O<sub>7-x</sub> multi-width no-insulation superconducting magnet *Supercond. Sci. Technol.* **29** 04LT04
- [10] Liu J *et al* 2020 World record 32.35 tesla direct-current magnetic field generated with an all-superconducting magnet *Supercond. Sci. Technol.* **33** 03LT01
- [11] Fazilleau P, Chaud X, Debray F, Lécresse T and Song J-B 2020 38 mm diameter cold bore metal-as-insulation HTS insert reached 32.5 T in a background magnetic field generated by resistive magnet *Cryogenics* **106** 103053
- [12] Yanagisawa Y *et al* 2016 27.6 T generation using Bi-2223/REBCO superconducting coils *IEEE CSC ESAS Supercond. News Forum Glob. Ed.* **21** 3599–603
- [13] Awaji S, Watanabe K, Oguro H, Miyazaki H, Hanai S, Tosaka T and Ioka S 2017 First performance test of a 25 T cryogen-free superconducting magnet *Supercond. Sci. Technol.* **30** 065001
- [14] Li Y, Park D, Yan Y, Choi Y, Lee J, Michael P C, Chen S, Qu T, Bascuñán J and Iwasa Y 2019 Magnetization and screening current in an 800 MHz (18.8 T) REBCO nuclear magnetic resonance insert magnet: experimental results and numerical analysis *Supercond. Sci. Technol.* **32** 105007
- [15] Kim J *et al* 2020 Design, construction, and operation of an 18 T 70 mm no-insulation (RE)Ba<sub>2</sub>Cu<sub>3</sub>O<sub>7-x</sub> magnet for an axion haloscope experiment *Rev. Sci. Instrum.* **91** 023314
- [16] Hahn S, Park D K, Bascunan J and Iwasa Y 2011 HTS pancake coils without turn-to-turn insulation *IEEE Trans. Appl. Supercond.* **21** 1592–5
- [17] Hahn S *et al* 2019 45.5-tesla direct-current magnetic field generated with a high-temperature superconducting magnet *Nature* **570** 496–9
- [18] Hu X, Rossi L, Stangl A, Sinclair J W, Kametani F, Abraimov D, Polyanskii A, Coulter J Y, Jaroszynski J and Larbalestier D C 2017 An experimental and analytical study of periodic and aperiodic fluctuations in the critical current of long coated conductors *IEEE Trans. Appl. Supercond.* **27** 1–5
- [19] Iwasa Y 2009 *Case Studies in Superconducting Magnets: Design and Operational Issues* (New York: Springer)
- [20] Gurevich A and Friesen M 2000 Nonlinear transport current flow in superconductors with planar obstacles *Phys. Rev. B* **62** 4004–25
- [21] Friesen M and Gurevich A 2001 Nonlinear current flow in superconductors with restricted geometries *Phys. Rev. B* **63** 064521
- [22] Zeldov E, Clem J R, McElfresh M and Darwin M 1994 Magnetization and transport currents in thin superconducting films *Phys. Rev. B* **49** 9802–22
- [23] Takahashi S, Suetomi Y, Takao T, Yanagisawa Y, Maeda H, Takeda Y and Shimoyama J 2020 Hoop stress modification, stress hysteresis and degradation of a REBCO coil due to the screening current under external magnetic field cycling *IEEE Trans. Appl. Supercond.* **30** 1–7
- [24] Kim S, Lee C, Bang J and Hahn S 2018 Manipulation of screening currents in an (RE)Ba<sub>2</sub>Cu<sub>3</sub>O<sub>7-x</sub> superconducting magnet *Mater. Res. Express* **6** 026004
- [25] Xia J, Bai H, Yong H, Weijers H W, Painter T A and Bird M D 2019 Stress and strain analysis of a REBCO high field coil based on the distribution of shielding current *Supercond. Sci. Technol.* **32** 095005
- [26] Yan Y, Xin C, Guan M, Liu H, Tan Y and Qu T 2020 Screening current effect on the stress and strain distribution in REBCO high-field magnets: experimental verification and numerical analysis *Supercond. Sci. Technol.* **33** 05LT02
- [27] Li Y, Park D, Lee W, Choi Y, Tanaka H, Bascuñán J and Iwasa Y 2020 Screening-current-induced strain gradient on REBCO conductor: an experimental and analytical study with small coils wound with monofilament and striated multifilament REBCO tapes *IEEE Trans. Appl. Supercond.* **30** 1–5
- [28] Abraimov D V, Feldmann D M, Polyanskii A A, Gurevich A, Liao S, Daniels G, Larbalestier D C, Zhuravel A P and Ustinov A V 2005 Imaging local dissipation and magnetic field in YBCO films with artificial defects *IEEE Trans. Appl. Supercond.* **15** 2954–7
- [29] Abraimov D, Feldmann D M, Polyanskii A A, Gurevich A, Daniels G, Larbalestier D C, Zhuravel A P and Ustinov A V 2004 Scanning laser imaging of dissipation in YBa<sub>2</sub>Cu<sub>3</sub>O<sub>7-δ</sub>-coated conductors *Appl. Phys. Lett.* **85** 2568–70